Adaptive Decoupling Switching Control of the Forced-Circulation Evaporation System Using Neural Networks

Yonggang Wang, Tianyou Chai, Jun Fu, Jing Sun, and Hong Wang

***Abstract*— For the forced-circulation evaporation process of alumina production, the control objectives include maintaining the liquid level and fast tracking of the product density with respect to its setpoint. However, with the strong coupling between the level control and product density control loops and the process exhibits strong nonlinearities, conventional control strategies, such as proportional-integral-derivative and other linear control design, cannot achieve satisfactory control performance and meet production demands. By augmenting the forced-circulation evaporation system model with dynamics of its operating valves, a nonlinear adaptive decoupling switching control strategy is proposed. This control strategy includes a linear adaptive decoupling controller, a neural-network-based nonlinear adaptive decoupling controller, and a switching mechanism. The linear adaptive decoupling controller is used to reduce the coupling between the two control loops. The neural-network-based nonlinear adaptive decoupling controller is employed to improve the transient performance and reduce the effects of the nonlinearities on the system, and the switching mechanism is introduced to guarantee the input–output stability of the closed-loop system. Simulation results show that the proposed method can decouple the loops effectively for the forced-circulation evaporation system and thus improve the evaporation efficiency.**

***Index Terms*— Adaptive decoupling control, dynamic model, forced-circulation evaporation system, switching control.**

I. Introduction

THE FORCED-CIRCULATION evaporation system is the final stage of the liquor burning process in the evaporation system associated with Bayer process for alumina production. The objective of the operation is to remove the organic impurities of the spent caustic liquor so that the liquor can be recycled. In order to improve the evaporation efficiency and to keep the production process smooth, large fluctuations of the liquid level of the evaporator should be avoided and the product density set point must also be tracked closely.

Level control and product density control of the forced-circulation system are challenging problems because of their inherent complex dynamics, high nonlinearity and strong coupling between the two loops [1]. Indeed, the decentralized control system cannot achieve satisfactory performance for the forced circulation evaporation system. Since the decentralized control method converts the multivariable system into several independent single control loops. It often results in large fluctuations in the liquor level, slow tracking of the product density setpoint, and can even lead to system instability.

In order to reduce the coupling between these control loops, several effective methods were proposed in the literature [1]–[7]. In [1]–[3], the input–output linearization decoupling technique based on differential geometry was proposed for the forced-circulation system and the five-effect evaporation system. In [4] and [5], the multivariable supervisory control method and the fuzzy control technique were applied to the falling film evaporator system. In [6] and [7], a model predictive control method was applied to an evaporation system. However, those methods did not take into account the dynamic characteristics of the control valves, which are not negligible. Moreover, parametric uncertainties of the evaporation system were not considered in the afore-mentioned literatures.

Over last decades, the effectiveness of adaptive decoupling control technology has been demonstrated in dealing with parameter uncertainties problems and coupled control loops [8]–[10]. However, since the linear adaptive decoupling controller is based on the linear models, their main drawback associated with these linear controllers is that they perform well only in a small neighborhood around certain operating point, and they cannot achieve desired performances for processes involving strong nonlinearities and large disturbances. On the other hand, research on combining adaptive control and neural networks has made significant progress in recent years [11]–[15]. However, its applications to complex systems such as the forced-circulation evaporation system have not been demonstrated, to the authors' best knowledge. By augmenting the forced-circulation evaporation system with the dynamics of the actuating valves, we propose an adaptive nonlinear decoupling switching controller using neural network in this brief so as to improve the closed-loop performance and the evaporation efficiency.

II. Forced-Circulation Evaporation System Description

The schematic diagram flow sheet of the forced-circulation evaporation system is shown in Fig. 1. The system is mainly composed of a flash tank, a pump, and the steam heaters. The symbols in Fig. 1 are explained as follows:

-C, -T	controller and instrument;
D, F, L	density, flow rate, level;
*	setpoint of relative control loop.

Manuscript received March 12, 2011; accepted March 7, 2012. Manuscript received in final form April 02, 2012. Date of publication May 1, 2012; date of current version April 17, 2013. This work was supported in part by the National Natural Science Foundation of China under Grant 61134006 and Grant 61020106003, the Chinese National Fundamental Research Program under Grant 2009CB320601, and the 111 Project of the Education Ministry of China under Grant B08015. Recommended by Associate Editor N. El-Farra.

Y. Wang, T. Chai, J. Fu, and H. Wang are with the State Key Laboratory of Synthetical Automation for Process Industry, Northeastern University, Shenyang 110819, China (e-mail: wygvern@gmail.com; tychai@neu.edu.cn; fujuncontrol@126.com; hong.wang@manchester.ac.uk).

J. Sun is with the Department of Electrical Engineering and Computer Science and the Department of Naval Architecture and Marine Engineering, University of Michigan, Ann Arbor, MI 48109 USA (e-mail: jingsun@umich.edu).

Color versions of one or more of the figures in this paper are available online at http://ieeexplore.ieee.org.

Digital Object Identifier 10.1109/TCST.2012.2193883

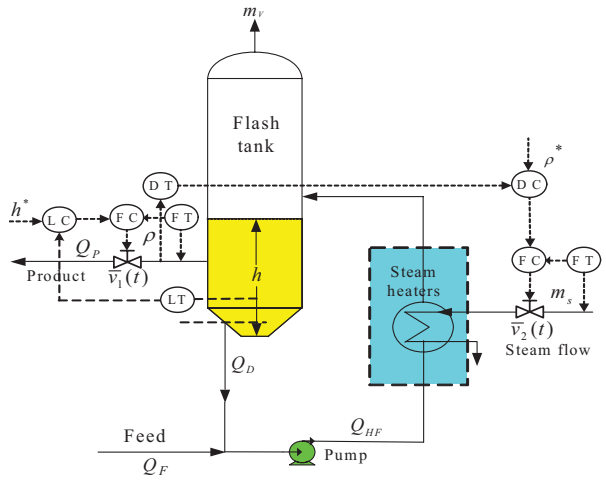

Fig. 1. Schematic chart of the forced-circulation evaporation system.

In this process, the feed flow (Q_F) is mixed with a high volumetric flow rate of recycling liquor (Q_D) and is pumped into a heat exchanger, which is heated by the steam. Then the liquid enters into the flash tank, where the liquid and the vapor are separated. The liquid is recycled with some drowned off as product. The vapor (m_V) is used as heating steam for other processes. The current control strategy of the forced-circulation system is accomplished by using mutli-loop cascade SISO controllers. The flow rate of the heat steam (m_s) is manipulated to control the product density (ρ), where the valve opening ($\bar{v}_2(t)$) is adjusted for the heat steam flow (m_s). The flash tank liquid level (h) is controlled by the discharge liquor flow (Q_P), where the valve opening ($\bar{v}_1(t)$) is adjusted for the discharge liquor flow (Q_P). Satisfactory performance is difficult to achieve using the conventional control strategy mainly for the following reasons. First, the two loops (the level control loop and product density tracking loop) have strong interactions and there are many disturbances, such as feed flow (Q_F) and feed density (ρ_f), in the forced-circulation system. Second, the parameters of specific heat of the liquor change with the different feed flow, and these changes lead to variations of dynamic characteristics of the forced-circulation system.

III. Augmented Plant of the Forced-Circulation System

A. Dynamic Modeling of the Forced-Circulation System

Assuming that the process was adiabatic, no flashing occurred in the heater and the specific heat capacities of all process streams are constants [2]. The dynamic modeling of the forced-circulation system can be derived from the mass and energy balances principles. In this context, the flash tank level can be derived from the material balance principles as follows [2]:

$$\frac{dh}{dt} = \frac{\left(Q_F - Q_P - \frac{m_V}{\rho_w}\right)}{A} \tag{1}$$

where Q_F is the feed flow rate, A is the cross-sectional area of the flash tank, m_V is the flash vapor mass, ρ_w is the density of the water, and h is the flash tank liquid level. The flash tank liquid product density can be derived from the mass balance principles as follows [2]:

$$\frac{d\rho}{dt} = \frac{(Q_F\rho_F(\rho/\rho_F - 1) - m_V(\rho/\rho_w - 1))}{(Ah)} \tag{2}$$

where ρ_F is the feed flow density and ρ is the production density. Flash tank liquid discharge temperature can be derived from the thermal balance principles as follows:

$$\frac{dT}{dt} = \frac{[Q_{HF}\rho_{HF}c_{HF}T_{HF} + \lambda_S m_s - m_V\lambda_v - (Q_{HF}\rho_{HF} - m_V)cT]}{(cAh\rho)} \tag{3}$$

where Q_{HF} is the heater feed rate, ρ_{HF} is the density of the heater feed, c_{HF} is the liquor heat capacity of the heater feed, T_{HF} is the temperature of the heater feed, λ_S is the latent heat of the heat steam, and λ_v is the latent heat of the vapor flash, where m_V, T_{HF}, and Q_{HF} are derived as follows:

$$m_V = \frac{(Q_F\rho_F c_F T_F - cQ_P\rho T + m_s\lambda_S)}{\lambda_V} \tag{4}$$

$$T_{HF} = \frac{(Q_F\rho_F c_F T_F + Q_D cT\rho)}{(Q_{HF}\rho_{HF}c_{HF})} \tag{5}$$

$$Q_{HF}\rho_{HF} = Q_D\rho + Q_F\rho_F \tag{6}$$

where Q_D is the recycling liquor flow, c_F is the liquor heat capacity of the feed, and c is the liquor heat capacity of the discharge.

B. Dynamic Modeling of the Control Valve

The valve opening can reflect the control inputs in actual process, it can verify whether the design of the controller is reasonable or not. Thus, the dynamics of actuating valves are considered in the controller design process in this brief. The model of the discharge flow, (where $\bar{v}_1$ and q_1 are input variable and output variable, respectively) and the model of the steam flow, (where $\bar{v}_2$ and q_2 are input variable and output variable, respectively) can be constructed using the process data. The dynamics of the above two valves can be described by the first-order plus dead-time models form as follows [16], [17]:

$$(T_i s + 1)q_i(s) = K_i e^{-L_i s}\bar{v}_i(s), \quad i = 1, 2, \ldots. \tag{7}$$

Using first-order Taylor expansion for the unknown time delays, i.e., $e^{-L_i s} = 1 - L_i s$, (7) becomes [16]

$$\int_0^t q_i(\tau)d\tau = -T_i q(t) + K_i \int_0^t v_i(\tau)d\tau - K_i L_i \bar{v}_i(t). \tag{8}$$

Equation (8) can be rewritten into a matrix form as

$$\gamma_i(t) = \phi_i^T(t)\theta_i \tag{9}$$

where $\gamma_i(t) = \int_0^t q_i(\tau)d\tau$, $\phi_i^T(t) = [-q_i(t), \int_0^t \bar{v}_i(\tau)d\tau, -\bar{v}_i(t)]$, $\theta_i^T = [-T_i, K_i, K_i L_i]$. This leads to

$$\Gamma_i = \Phi_i\theta_i \tag{10}$$

where $\Gamma_i = [\gamma(t_1), \gamma(t_2), \ldots, \gamma(t_N)]^T$, $\Phi_i = [\phi(t_1), \phi(t_2), \ldots, \phi(t_N)]^T$. Its least squares estimation for θ are given by

$$\hat{\theta}_i = [\Phi_i^T\Phi_i]^{-1}\Phi_i^T\Gamma_i. \tag{11}$$

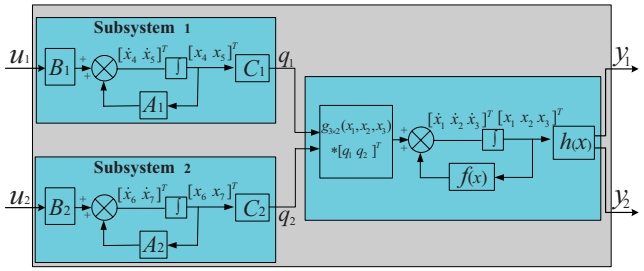

Fig. 2. Chart of the augmented plant for the forced-circulation evaporation system.

Using (8)–(11), the model of the discharge flow and steam flow can be obtained as follows:

$$\frac{q_1(s)}{\bar{v}_1(s)} = \frac{1.74}{(5.28s+1)} \quad \frac{q_2(s)}{\bar{v}_2(s)} = \frac{0.3}{(4.68s+1)}. \tag{12}$$

C. Augmented Plant Model

Substituting (4)–(6) into (1)–(3) yields the following dynamic model without actuators' dynamics for the system, (13)–(15), as shown in the bottom of the page.

In this section we describe the augmented plant of the evaporation system by including by two subsystems that represent the valve dynamics. The block diagram of the augmented plant dynamic model for the forced-circulation evaporation system is shown in Fig. 2.

According to dynamic models of control valves (12), the proportional-integral-derivative (PID) controller parameters are acquired as follows: $K_p1 = 0.9976$; $K_i1 = 0.1903$, $K_d1 = 0$, $K_p2 = 4.9131$; $K_i2 = 1.1789$; and $K_d2 = 0$. Substituting the PID controller into the dynamic model, the close-loop equation can be obtained as follows:

$$\frac{q_1(s)}{u_1(s)} = \frac{(0.3288s+1.7276)}{(s^2+0.5181s+1.7276)} \tag{16}$$

$$\frac{q_2(s)}{u_2(s)} = \frac{(0.3149s+0.2671)}{(s^2+0.5286s+0.2671)} \tag{17}$$

where q_1 and q_2 are the discharge flow and the steam flow, respectively, u_1 and u_2 are the discharge flow setpoint and steam flow setpoint, respectively.

Define $h = x_1$, $\rho = x_2$, and $T = x_3$. Equations (16) and (17) can be transformed into the following state space form:

$$[\dot{x}_4\ \dot{x}_5]^T = [0\ 1;-1.7276-0.5181;][x_4\ x_5]^T+[0\ 1]^T u_1 \tag{18}$$

$$q_1 = [1.7276\ 0.3288][x_4\ x_5]^T \tag{19}$$

$$[\dot{x}_6\ \dot{x}_7]^T = [0\ 1;-0.2671-0.5288;][x_6\ x_7]^T+[0\ 1]^T u_2 \tag{20}$$

$$q_2 = [0.2671\ 0.3149][x_6\ x_7]^T. \tag{21}$$

Substituting (19), (21) into (13)–(15) and combining the result with (18) and (20), we can derive the augmented plant as follows:

$$\begin{cases} \dot{x}_1 = \frac{1}{A\rho_w\lambda_V}[Q_F(\rho_w\lambda_V - \rho_F c_F T_F) - (\rho_w\lambda_V - cx_2x_3) \\ (1.7276x_4 + 0.3288x_5) - \lambda_S(0.2671x_6 + 0.3149x_7)] \\ \dot{x}_2 = \frac{1}{A\lambda_V\rho_w x_1}[Q_F\lambda_V\rho_w x_2 - Q_F\lambda_V\rho_w\rho_F - (Q_F\rho_F c_F T_F \\ \quad -cx_2x_3(1.7276x_4 + 0.3288x_5) + \lambda_s(0.2671x_6 \\ \quad + 0.3149x_7))(x_2 - \rho_w)] \\ \dot{x}_3 = \frac{1}{A\lambda_V x_1 x_2}[Q_F\rho_F(c_F T_F - \lambda_V)x_3 + (\lambda_V - cx_3)x_2x_3 \\ (1.7276x_4 + 0.3288x_5) + \lambda_s x_3(0.2671x_6 + 0.3149x_7)] \\ \dot{x}_4 = x_5 \\ \dot{x}_5 = -1.7276x_4 - 0.5181x_5 + u_1 \\ \dot{x}_6 = x_7 \\ \dot{x}_7 = -0.2671x_6 - 0.5288x_7 + u_2. \end{cases} \tag{22}$$

Equation (22) can be written as

$$\dot{x} = f(x_1, x_2, x_3, x_4, x_5, x_6, x_7) + Bu(t) \tag{23}$$

where $u(t) = [u_1(t)u_2(t)]^{\mathrm{T}}$, $B = \left[\begin{smallmatrix} 0&0&0&0&1&0&0 \\ 0&0&0&0&0&0&1 \end{smallmatrix}\right]$, and $x(t) = [x_1(t)\ x_2(t)\ x_3(t)\ x_4(t)\ x_5(t) x_6(t)\ x_7(t)]^{\mathrm{T}}$ with system outputs given by $y(t) = Cx(t)$ where

$$C = \begin{bmatrix} 1&0&0&0&0&0&0 \\ 0&1&0&0&0&0&0 \end{bmatrix} y(t) = \left[y_1(t)\ y_2(t)\right]^{\mathrm{T}}.$$

Actually, the subsystem is composed of valve dynamic model and the PID controller. From a control engineering point of view, the augmented dynamic model of the evaporation system corresponds to a classical cascade feedback control system. The inner loops correspond to the fast dynamics, which is associated to the actuators, and the outer loop corresponds to the control of the evaporation system, which is described by a nonlinear dynamic model. The augmented plant consists of the subsystem and the evaporation system information. Thus, it can effectively improve the control performance.

D. Estimation of Model Parameters

Several model parameters are directly measurable, such as feed flow Q_F, and feed temperature T_F, etc. Cross-sectional area of flash tank A can be determined from the physical parameters of the forced-circulation system. Latent heat λ_S and λ_v can be obtained from the saturated steam table. The parameters of liquor heat capacity c and c_F are the two major parameters whose identification constitutes a challenging problem. This is because the parameters of the liquor heat capacity can neither be directly measured nor determined indirectly from other variables.

According to (13)–(15), the forced-circulation process with the unknown parameters of the liquor heat capacity can be

$$\frac{dh}{dt} = \frac{[Q_F(\rho_w\lambda_V - \rho_F c_F T_F) - \rho_w\lambda_V Q_P + cT\rho Q_P - \lambda_S m_s]}{(A\rho_w\lambda_V)} \tag{13}$$

$$\frac{d\rho}{dt} = \frac{[Q_F\lambda_V\rho_w\rho - Q_F\lambda_V\rho_w\rho_F - (Q_F\rho_F c_F T_F - cT\rho Q_P + \lambda_s m_s)(\rho - \rho_w)]}{(A\lambda_V\rho_w h)} \tag{14}$$

$$\frac{dT}{dt} = \frac{[Q_F\rho_F(c_F T_F - \lambda_V)T + (\lambda_V - cT)\rho T Q_P + \lambda_s T m_s]}{(A\lambda_V h\rho)} \tag{15}$$

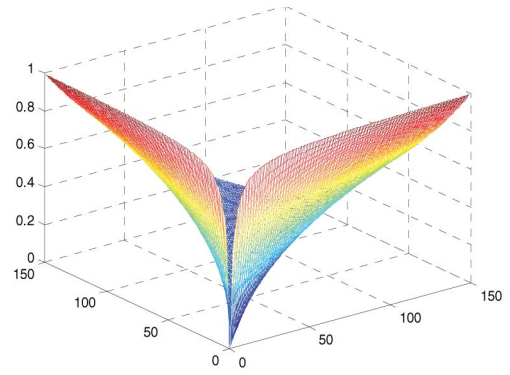

Fig. 3. Gap-matrix surface of the forced-circulation process.

written as

$$\dot{x} = f(x,\theta) + g(x,\theta)\bar{u}(t) \tag{24}$$

$$y(t) = \bar{C}x(t) \tag{25}$$

where $\theta = [c_f \quad c]$, $x = [x_1 \; x_2 \; x_3]^T$, $\bar{C} = [1 \; 0; 0 \; 1;]$, $\bar{u}(t) = [Q_p, m_s]^T$. As it can be seen from (24) and (25), the parameter estimation is a challenging problem because of the model nonlinearity in the system. Indeed, it is a nonlinear parameter estimation problem in nature. The aim of the parameter estimation is to estimate the parameter vector $\hat{\theta}$ in such a way that response deviation of the system $y(t)$ and the model output $\hat{y}(t,\theta)$ becomes minmal. The objective function can be formulated as

$$\min \xi(\theta) = \sum_{j=1}^{n} \left(\left[y_j(t) - \hat{y}_j(t,\theta) \right] \left[y_j(t) - \hat{y}_j(t,\theta) \right]^T \right) \tag{26}$$

where $y(t)$ and $\hat{y}(t,\theta)$ are the system and model output samples at time t, respectively, and N the number of samples. In this brief, the genetic algorithm (GA) is used to solve the above optimization [18], [19]. The parameter values for the forced-circulation system are obtained as follows:

$$\begin{aligned} Q_F &= 80 \text{ m}^3/\text{h}, A = 40 \text{ m}^2, T_F = 100 \text{ °C}, \\ \lambda_S &= 2185 \text{ kJ/kg}, \rho_F = 1365 \text{ kg/m}^3, \\ \lambda_V &= 2247 \text{ kJ/kg}, c_F = 3.61 \text{ kJ/(kg} \cdot \text{°C)}, \\ c &= 3.6 \text{ kJ/(kg} \cdot \text{°C)}, \rho_w = 1000 \text{ kg/m}^3. \end{aligned}$$

E. Analysis of the System Dynamic Behavior

To investigate process dynamic behavior, the strong nonlinearity characteristic, uncertain parameters of the system are subsequently introduced in this section.

1) Gap-Metric-Based Nonlinearity Measure for the Forced-Circulation Process: Recently, a nonlinearity measure via gap metric is proposed to assess the nonlinearity of the nonlinear system [20], [21]. Grid the operating space of the forced-circulation by N operating points, and the nonlinearity measure is defined as [21]

$$\upsilon = \max_{i,j=1,2\ldots N} \{\delta(L_i NL, L_j NL\} \tag{27}$$

where $L_i NL$, $L_j NL$ are linearization systems of the nonlinear plant at the i-th and the j-th operating point, respectively. The value of υ is bounded between 0 and 1. The process has strong nonlinearity if υ is close to 1. In this case, the linearized system of the nonlinear system would behave quite differently, namely, the dynamics of the nonlinear system in the operating space are rather inconsistent. A single linear controller may not be sufficient to achieve satisfactory performance for the nonlinear system over the entire the operating range, and a nonlinear controller is necessary [21]. On the other hand, the process could be approximated by a linear system if υ is close to 0. In this case, the linearized system in the operating space have similar dynamics, that is to say, the dynamic of the nonlinear system are basically the same in the operating space.

The nonlinearity measure υ of the forced-circulation system can be calculated by (27) as follows. Since the ranges of the variables for the process are $x_1 \in [2,3]$, $x_2 \in [1429.4, 1449]$, $u_1 \in [68, 72.5]$, and $u_2 \in [11.2, 15.7]$. We can grid the above operating space using 150 operating points and linearize the nonlinear system around these 150 points. Then 150 linear systems are formulated. The gag metric values are computed between the 150 linear systems. Compared with the $N \times N$ gaps, the biggest one are chosed as the nonlinearity measure υ. The gaps are shown in Fig. 3.

As it can be seen from Fig. 3, the measure $\upsilon = 1$. The result shows that the dynamics of the forced-circulation system is quite different at different operating points within its operating range. The process has strong nonlinearity in the operating space and the nonlinear control strategy is required.

2) Uncertainties Parameters Effect to the Forced-Circulation Process: In most previous research on evaporation system, researchers always treated the c_F as known and fixed parameter. However, in reality, the parameter c_F is very difficult to be obtained precisely and its value changes with the different operation conditions. Therefore parameter c_F is really uncertain. In order to further illustrate the impact of the unknown parameter c_F on the system, let us consider the experiment with different liquor heat capacity c_F in the steady-state, $c_F = 3.63, 3.65$. The product density (ρ) and the liquid level (h) response can be seen from Fig. 4.

As can be seen from Fig. 4, product density (ρ) and the liquid level (h) exhibit large sensitivity even to small variation in parameter c_F. Furthermore, it can be seen from (13)–(15) that any variation in the control inputs (Q_P, m_s) will affect both system outputs (h, ρ). The evaporator system shows strong interactions between the two loops [22], [23]. Therefore, it is a challenging issue to propose a nonlinear adaptive control method that can be used in forced-circulation system with unknown nonlinear parameter c_F (that affects the system dynamics in a nonlinear fashion), strong nonlinearity and strong coupling characteristics.

F. Model Validation

The goal of model validation is to establish the validity of the dynamic model described in this brief with chosen the proper parameters. In this process, we collect the measured input data and output data from the actual industrial process. Then the model response is generated using the same actual

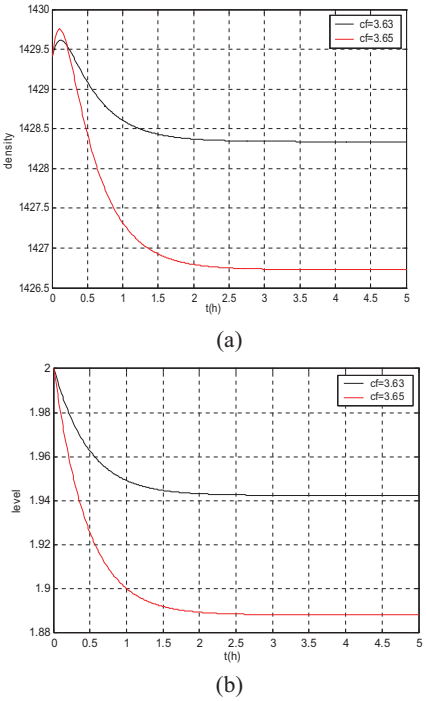

Fig. 4. Simulation results with different unknown parameters c_F. (a) Product density response. (b) Liquid level response.

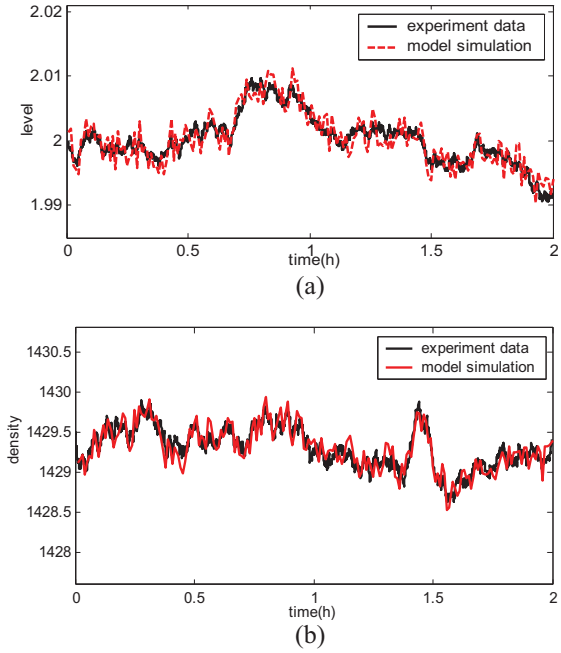

Fig. 5. Model validation results.

control input data. If the two responses match adequately, a validated model is obtained.

The model validation results are shown in Fig. 5, where the predicted tank level and the discharge density are compared with the measured data from the actual process. In this brief, root mean squared error (RMSE) is used to determine goodness of fit. The validation results in a RMSE of 0.26 cm and 0.28 kg/m^3 for the tank level and the discharge density, respectively.

As it can be seen from Fig. 5, the model's predictions of tank level and the discharge density track the observed trends rather well and the actual system dynamics are correctly "captured." Thus the dynamic model of the forced-circulation system is thus accepted as a reasonable approximation of the actual process and model prediction capability of the forced-circulation system will be assumed properly for the purposes of this simulation study.

IV. Nonlinear Adaptive Decoupling Switching Control Strategy

Discrete model of the augmented plant can be acquired via the Euler method by selecting the sampling period T and the model can be transformed into the NARMA form as follows:

$$y_1(k+1) = f_{y1}(y_1(k), y_1(k-1), y_2(k), y_2(k-1), u_1(k), u_1(k-1), u_2(k), u_2(k-1)) \quad (28)$$

$$y_2(k+1) = f_{y2}(y_1(k), y_1(k-1), y_2(k), y_2(k-1), u_1(k), u_1(k-1), u_2(k), u_2(k-1)). \quad (29)$$

Equations (28) and (29) can be rewritten as a general form

$$y(k) = f[y(k-1), \ldots, y(k-n_a), u(k-1), \ldots, u(k-n_b-1)] \quad (30)$$

where $u(k) = \left[u_1(k)\ u_2(k)\right]^{\mathrm{T}} \in \mathbf{R}^2$ denotes the discharge flow setpoint and steam flow setpoint. $y(k) = \left[y_1(k)\ y_2(k)\right]^{\mathrm{T}} \in \mathbf{R}^2$ is the system outputs. $f[\cdot] \in R^2$ is a smooth vector-valued nonlinear function, n_a and n_b are the system orders.

The augmented plant of the forced-circulation system can be decomposed into a linear model incorporating a nonlinear term around the operating point as expressed in the following formulation [24]:

$$\begin{bmatrix} y_1(k) \\ y_2(k) \end{bmatrix} = -\begin{bmatrix} a_{11}(z^{-1}) & 0 \\ 0 & a_{22}(z^{-1}) \end{bmatrix} \begin{bmatrix} y_1(k-1) \\ y_2(k-1) \end{bmatrix} + \begin{bmatrix} b_{11}(z^{-1}) & b_{12}(z^{-1}) \\ b_{21}(z^{-1}) & b_{22}(z^{-1}) \end{bmatrix} \begin{bmatrix} u_1(k-1) \\ u_2(k-1) \end{bmatrix} + \begin{bmatrix} v_1(k-1) \\ v_2(k-1) \end{bmatrix} \quad (31)$$

where $a_{ii}(z^{-1})$ and $b_{ij}(z^{-1})$ are polynomial about z^{-1}. $v(k-1) = v[y(k-1), \ldots, y(k-n_a), u(k-1), \ldots, u(k-n_b-1)] \in R^2$ is the higher order nonlinear item.

Equation (31) can be rewritten as follows:

$$A(z^{-1})y(k) = \bar{B}(z^{-1})u(k-1) + \bar{\bar{B}}(z^{-1})u(k-1) + v(k-1) \quad (32)$$

where

$$A(z^{-1}) = \begin{bmatrix} 1 + z^{-1}a_{11}(z^{-1}) & 0 \\ 0 & 1 + z^{-1}a_{22}(z^{-1}) \end{bmatrix}$$

$$\bar{B}(z^{-1}) = \begin{bmatrix} b_{11}(z^{-1}) & 0 \\ 0 & b_{22}(z^{-1}) \end{bmatrix}$$

$$\bar{\bar{B}}(z^{-1}) = \begin{bmatrix} 0 & b_{12}(z^{-1}) \\ b_{21}(z^{-1}) & 0 \end{bmatrix}.$$

Remark 1: Considering the physical restrictions of the forced-circulation process, the nonlinear term $v(k-1)$ is assumed to be bounded in this brief.

A. Nonlinear Decoupling Controller

In order to decouple the control loops and eliminate the influence of the nonlinear term for the forced-circulation process, the following performance index adopted by [24] is introduced based on generalized predictive control law:

$$J = \sum_{j=1}^{N} ||y(k+j) - r_j w(k+j) + S_j(z^{-1})u(k+j-1) + K_j(z^{-1})v(k+j-1)||^2_{\lambda_j} + \sum_{j=1}^{N} ||u(k+j-1)||^2_{Q_j(z^{-1})} \tag{33}$$

where N denotes a prediction range, r_j and λ_j are diagonal weighted matrices, $K_j(z^{-1})$ is a diagonal polynomial matrix about z^{-1}, $S_j(z^{-1})$ is a polynomial matrix with zero diagonal elements that can eliminate coupling, $Q_j(z^{-1})$ are diagonal weighted matrices as expressed in the following formulation:

$$\begin{aligned} Q_j(z^{-1}) &= \text{diag}[q_0^{j1} q_0^{j2}]_{2\times 2} j = 2, 3, \ldots, N \\ Q_1(z^{-1}) &= \text{diag}[q_0^{11} + q_1^1 z^{-1} + \cdots q_{m_1}^1 z^{-m_1} q_0^{12} + q_1^2 z^{-1} \\ &\quad + \cdots q_{m_2}^2 z^{-m_2}]_{2\times 2} \\ &= \text{diag}[q_0^{11} + z^{-1} Q_{11}(z^{-1}) q_0^{12} + z^{-1} Q_{12}(z^{-1})]_{2\times 2} \end{aligned}$$

where $Q_1(z^{-1})$ is a diagonal polynomial matrix about z^{-1}, $Q_j(z^{-1}), j = 1, \ldots, N$ are diagonal constant matrices. In order to obtain j-step ahead predictor, we introduce the following Diophantine equations:

$$I = E_j(z^{-1})A(z^{-1}) + z^{-j}F_j(z^{-1}) \tag{34}$$

$$E_j(z^{-1})\bar{B}(z^{-1}) = G_j(z^{-1}) + z^{-j}H_j(z^{-1}) \tag{35}$$

$$E_j(z^{-1})\bar{\bar{B}}(z^{-1}) = \bar{\bar{G}}_j(z^{-1}) + z^{-j}\bar{\bar{H}}_j(z^{-1}) \tag{36}$$

where $E_j(z^{-1}), F_j(z^{-1}), G_j(z^{-1}), H_j(z^{-1})$ are diagonal polynomial matrices about z^{-1}, $\bar{\bar{G}}_j(z^{-1}), \bar{\bar{H}}_j(z^{-1})$ are polynomial matrices with zero diagonal elements as expressed in the following formulation:

$$\begin{aligned} E_j(z^{-1}) &= \sum_{i=0}^{j-1} E_i z^{-i}, F_j(z^{-1}) = \sum_{i=0}^{n_a-1} F_i z^{-i} \\ G_j(z^{-1}) &= \sum_{i=0}^{j-1} G_i z^{-i}, H_j(z^{-1}) = \sum_{i=0}^{n_b-1} H_i z^{-i} \\ \bar{\bar{G}}_j(z^{-1}) &= \sum_{i=0}^{j-1} \bar{\bar{G}}_i z^{-i}, \bar{\bar{H}}_j(z^{-1}) = \sum_{i=0}^{n_b-1} \bar{\bar{H}}_i z^{-i}. \end{aligned}$$

With (32), (34)–(36), j-step ahead predictor can be given by

$$\begin{aligned} y(k+j) = {} & F_j(z^{-1})y(k) + G_j(z^{-1})u(k+j-1) \\ & + H_j(z^{-1})u(k-1) + \bar{\bar{G}}_j(z^{-1})u(k+j-1) \\ & + \bar{\bar{H}}_j(z^{-1})u(k-1) + E_j(z^{-1})v(k+j-1). \end{aligned} \tag{37}$$

In this context, $S_j(z^{-1})$ and $K_j(z^{-1})$ can be selected to satisfy

$$\begin{aligned} & S_j(z^{-1})u(k+j-1) + \bar{\bar{G}}_j(z^{-1})u(k+j-1) \\ & \quad + \bar{\bar{H}}_j(z^{-1})u(k-1) = \bar{\bar{M}}_j(z^{-1})u(k-1) \\ & [E_j(z^{-1}) + K_j(z^{-1})]v(k+j-1) = \bar{E}_j(z^{-1})v(k-1) \end{aligned}$$

where $\bar{\bar{M}}_j(z^{-1})$ are polynomial matrices with zero diagonal elements. Substituting $y(k+j)$ into the performance index yields

$$\begin{aligned} J = {} & \sum_{j=1}^{N} ||F_j(z^{-1})y(k) + G_j(z^{-1})u(k+j-1) \\ & + H_j(z^{-1})u(k-1) + \bar{\bar{M}}_j(z^{-1})u(k-1) - r_j w(k+j) \\ & + \bar{E}_j(z^{-1})v(k-1)||^2_{\lambda_j} + \sum_{j=1}^{N} ||u(k+j-1)||^2_{Q_j(z^{-1})}. \end{aligned} \tag{38}$$

Minimizing the cost function J with respect to U leads to

$$\begin{aligned} U = (G^T\lambda G + Q_0)^{-1} \Big\{ & G^T\lambda[RW - Fy(k) - Hu(k-1) \\ & - \bar{\bar{M}}u(k-1) - \bar{E}v(k-1)] - \sum_{i=1}^{m} Q_i z^{-i} U \Big\} \end{aligned} \tag{39}$$

where $Q_0 = \text{diag}[q_0^{11}, q_0^{12}, q_0^{21}, q_0^{22}, \ldots, q_0^{N1}, q_0^{N2}]$, and $Q_i = \text{diag}[q_i^1, \ldots, q_i^2, 0, \ldots, 0]$, $i = 1, \ldots, m, m = \max[m_1\ m_2]$. G is the lower triangular Toeplitz matrix, which are the coefficients of $G_j(z^{-1})$. Let $P = [P_1, P_2, \ldots, P_N]$ be the first two rows of $(G^T\lambda G + Q_0)^{-1}G^T\lambda$, and $P' = [P'_1, P'_2, \ldots, P'_N,]$ be the first two rows of $(G^T\lambda G + Q_0)^{-1}$, where P_i $(i = 1, \ldots, N)$ and P'_i $(i = 1, \ldots, N)$ are 2×2 diagonal matrixes. Then it can be obtained that

$$\begin{aligned} u(k) = {} & P^*[RW - Fy(k) - Hu(k-1) - \bar{\bar{M}}u(k-1) \\ & - \bar{E}v(k-1)] - P'^*_1 Q'_1(z^{-1})u(k-1) \end{aligned} \tag{40}$$

where $Q'_1(z^{-1}) = \text{diag}[Q_{11}(z^{-1}) \quad Q_{12}(z^{-1})]_{2\times 2}$. We define

$$\begin{aligned} R_c &= \sum_{i=1}^{N} P_i R_i;\ F_c(z^{-1}) = \sum_{k=1}^{N} P_k F_k(z^{-1}) \\ H_c(z^{-1}) &= \sum_{k=1}^{N} P_k H_k(z^{-1});\ \bar{\bar{M}}_c(z^{-1}) = \sum_{k=1}^{N} P_k \bar{\bar{M}}_k(z^{-1}) \\ E_c(z^{-1}) &= \sum_{k=1}^{N} P_k \left[E_k(z^{-1}) + K_k(z^{-1})\right] Q_c(z^{-1}) = P'^*_1 \\ & \quad \text{diag}\left[q_1^1 q_1^2\right]_{2\times 2} + P'^*_1 \text{diag}[q_2^1 z^{-1} \cdots q_2^2 z^{-1}]_{2\times 2} \\ & \quad + \cdots P'^*_1 \text{diag}[q_m^1 z^{-m_1+1} q_m^2 z^{-m_2+1}]_{2\times 2}. \end{aligned}$$

Equation (40) can be written as

$$\begin{aligned} u(k) = {} & R_c w(k) - F_c(z^{-1})y(k) - H_c(z^{-1})u(k-1) \\ & - \bar{\bar{M}}_c(z^{-1})u(k-1) - Q_c(z^{-1})u(k-1) - E_c(z^{-1})v(k) \end{aligned} \tag{41}$$

where $H_c(z^{-1})$ and $Q_c(z^{-1})$ are diagonal polynomial matrices. Define $I + z^{-1}H_c(z^{-1}) + z^{-1}Q_c(z^{-1}) = \bar{H}_c(z^{-1})$. Equation (41) can be given by

$$\begin{aligned} \bar{H}_c(z^{-1})u(k) = {} & R_c w(k) - F_c(z^{-1})y(k) - \bar{\bar{M}}_c(z^{-1})u(k-1) \\ & - E_c(z^{-1})v(k-1) \end{aligned} \tag{42}$$

where $\bar{H}_c(z^{-1}), F_c(z^{-1})$, and $E_c(z^{-1})$ are diagonal polynomial matrices, R_c is diagonal constant matrix, $\bar{\bar{M}}_c(z^{-1})$ is a

polynomial matrix with zero diagonal elements. The nonlinear generalized predictive decoupling controller (42) is composed of three parts: namely a generalized predictive controller, a decoupling compensator and a nonlinear compensator. In this context, the generalized predictive controller can be used to realize asymptotical tracking of the output $y(k)$ with respect to a specified bounded signal $w(k)$. The nonlinear compensator is used to eliminate the influence of the nonlinear term $v(\cdot)$ to the controlled output. The decoupling compensator is designed to decouple the control loops.

By substituting (42) into (32), the closed-loop system equation can be expressed as

$$\left\{z^{-1}F_c\left(z^{-1}\right)B\left(z^{-1}\right)+A\left(z^{-1}\right)\left[\bar{H}_c\left(z^{-1}\right)+z^{-1}\bar{\bar{M}}_c\left(z^{-1}\right)\right]\right\}u(k) = R_cA\left(z^{-1}\right)w(k)-\left[A\left(z^{-1}\right)E_c\left(z^{-1}\right)+z^{-1}F_c\left(z^{-1}\right)\right]v(k-1). \tag{43}$$

From (43), it can be seen that matrices $F_c(z^{-1})$, $\bar{H}_c(z^{-1})$, and $z^{-1}\bar{\bar{M}}_c(z^{-1})$ are related to the diagonal weighted matrices λ and $Q_c(z^{-1})$. Therefore, to guarantee the stability of the system, λ and $Q_c(z^{-1})$ should be chosen to satisfy the following condition:

$$\det T(z^{-1}) = \det\left\{z^{-1}F_c(z^{-1})B(z^{-1})+A(z^{-1}) \times\left[\bar{H}_c(z^{-1})+z^{-1}\bar{\bar{M}}_c(z^{-1})\right]\right\}\neq 0, \quad |z|>1. \tag{44}$$

In order to choose the other weighting polynomials, substituting (42) into (32) yields the following equation:

$$\begin{aligned}&\left[\bar{H}_c(z^{-1})A(z^{-1})+z^{-1}F_c(z^{-1})\bar{B}(z^{-1})\right]y(k+1)\\ &=\bar{B}(z^{-1})R_cw(k)\\ &\quad+\left[\bar{H}_c(z^{-1})\bar{\bar{B}}(z^{-1})\ -z^{-1}\bar{B}(z^{-1})\bar{\bar{M}}_c(z^{-1})\right]u(k)\\ &\quad+\left[\bar{H}_c(z^{-1})\ -\bar{B}(z^{-1})E_c(z^{-1})\right]v(k).\end{aligned} \tag{45}$$

From (45), the tracking errors, the coupling and the effect of the unmodeled dynamics can be eliminated in the steady-state of the closed-loop system, provided that the matrices $F_c(z^{-1})$, $\bar{\bar{M}}_c(z^{-1})$, and R_c satisfy

$$\bar{H}_c(1)A(1)+z^{-1}F_c(1)\bar{B}(1) = \bar{B}(1)R_c \tag{46}$$

$$\bar{H}_c(1)\,\bar{\bar{B}}(1) = \bar{B}(1)\,\bar{\bar{M}}_c(1) \tag{47}$$

$$\bar{H}_c(1) = \bar{B}(1)\,E_c(1). \tag{48}$$

As it can be seen from (42) that the linear generalized predictive decoupling controllers can be obtained as

$$\bar{H}_c(z^{-1})u(k) = R_cw(k)-F_c(z^{-1})y(k)-\bar{\bar{M}}_c(z^{-1})u(k-1). \tag{49}$$

The linear generalized predictive decoupling controllers can be applied to the controlled plant when the nonlinear term $v(t)$ of the system is small and negligible. The nonlinear generalized predictive decoupling controllers should be applied to the plant when the system has strong nonlinearity.

Remark 2: Because of the existence of the uncertainties of parameter c_F in the forced-circulation system, the nonlinear decoupling controller in [25] does not work well. This brief introduces a nonlinear adaptive decoupling control strategy, which aims to address the problems associated with parameter uncertainties for the nonlinear systems. Furthermore, the controller design in this brief is based on generalized predictive control law rather than generalized minimum variance law. Thus the parameters selection method in this brief is different from that in [25].

B. Adaptive Decoupling Switching Control Based on Neural Networks

According to (32), the identification equation of system parameters is

$$y(k) = \Theta^TX(k-1)+v(k-1) \tag{50}$$

where $\Theta = [A_1,\ldots,A_{n_a},B_0,\ldots,B_{n_b}]^T$, $X(k-1)=[-y^T(k-1),\ldots,-y^T(k-n_a),u^T(k-1),\ldots,u^T(k-n_b-1)]^T$.

In this brief, two estimation models are used to predict the output of the system. The first one is the linear estimation model

$$\hat{y}_1(k) = \hat{\Theta}_1^T(k-1)X(k-1) \tag{51}$$

where $\hat{\Theta}_1^T(k-1)$ is an estimation of Θ at instant k–1. The parameter matrix Θ is identified by the following algorithm:

$$\hat{\Theta}_1(k) = \hat{\Theta}_1(k-1)+\frac{\mu_1(k)X(k-1)e_1^T(k)}{1+X(k-1)^TX(k-1)} \tag{52}$$

$$\mu_1(k) = \begin{cases}1, & \text{if } \|e_1(k)\|>4\Delta\\ 0, & \text{else}\end{cases} \tag{53}$$

where $\Delta>0$ is the upper bound of the nonlinear term $v(k-1)$.

$e_1(k)$ is the linear model error

$$e_1(k) = y(k)-\hat{y}_1(k) = y(k)-\hat{\Theta}_1^T(k-1)X(k-1). \tag{54}$$

The second one is the neural network nonlinear estimation model given by

$$\hat{y}_2(k) = \hat{\Theta}_2^T(k-1)X(k-1)+\hat{v}(k-1) \tag{55}$$

where $\hat{v}(k-1)$ can be estimated by multilayer neural networks [26] and $\hat{\Theta}_2^T(k-1)$ is another estimation of Θ at instant k–1. The parameter matrix Θ is identified by the following algorithm:

$$\hat{\Theta}_2(k) = \hat{\Theta}_2(k-1)+\frac{\mu_2(k)X(k-1)e_2^T(k)}{1+X(k-1)^TX(k-1)} \tag{56}$$

$$\mu_2(k) = \begin{cases}1, & \text{if } \|e_2(k)\|>4\Delta\\ 0, & \text{else}\end{cases} \tag{57}$$

where $\Delta>0$ is the upper bound of the nonlinear term $v(k-1)$.

$e_2(t)$ is the nonlinear model error, i.e.,

$$e_2(k)=y(k)-\hat{y}_2(k)=y(k)-\hat{\Theta}_2^T(k-1)X(k-1)-\hat{v}(k-1). \tag{58}$$

If nonlinear item $\hat{v}_(k-1)$ is not considered, the linear adaptive decoupling control law based on the linear estimation model is obtained as

$$\hat{\bar{H}}_{1c}(z^{-1})u(k) = \hat{R}_{1c}w(k)-\hat{F}_{1c}(z^{-1})y(k)-\bar{\bar{M}}_{1c}(z^{-1})u(k-1). \tag{59}$$

From (42), the nonlinear adaptive decoupling control law based on the neural network nonlinear estimation model is obtained as

$$\hat{\bar{H}}_{2c}(z^{-1})u(k) = \hat{R}_{2c}w(k) - \hat{F}_{2c}(z^{-1})y(k) - \bar{\bar{M}}_{2c}(z^{-1})u(k-1) - \hat{E}_c(z^{-1})\hat{v}(k-1). \quad (60)$$

The linear adaptive decoupling controller can guarantee the stability of the close-loop system. However, it does not consider effects of the nonlinearities on the system output. The performance of control system becomes poor when $\hat{v}(k-1)$ is larger. The nonlinear adaptive decoupling controller can reduce the impact of nonlinearity on system output. But it cannot guarantee the stability of the close-loop system. In order to improve performance of control system and ensure the stability for the closed-loop system, a switching mechanism is introduced. The switching criterion is defined as

$$J_i(k) = \sum_{l=1}^{k} \frac{\mu_i(l)(||e_i(l)||^2 - 16\Delta^2)}{4(1 + X(l-1)^T X(l-1))} + \alpha \sum_{l=k-N+1}^{k} (1 - \mu_i(l))||e_i(l)||^2 \quad (i = 1, 2) \quad (61)$$

$$\mu_i(k) = \begin{cases} 1, & \text{if } \|e_i(k)\| > 4\Delta \\ 0, & \text{else} \end{cases} \quad (62)$$

where N is an integer and $\alpha \geq 0$ is a predefined constant. $i = 1$ stands for the linear model, $i = 2$ denotes the nonlinear models. At each time instant k, the linear estimation model and the nonlinear model predict the system output, and the parameters of models are updated through the input–output data. At the same time, we calculate $J_1(k)$, $J_2(k)$, and choose the control law $u^*(t)$ corresponding to the smaller $J^*(k)$ to be applied to the system.

Theorem 1: When the adaptive control algorithm (52)–(54) and (56)–(58) and the switching mechanism (61) are applied to the system, the input and output signals of the closed-loop system are bounded, i.e., $||y(k)|| < \infty$, $||u(k)|| < \infty$. Moreover, the generalized tracking error of the closed-loop system satisfies

$$\lim_{k\to\infty} ||\bar{e}(k)|| = \lim_{k\to\infty} ||\hat{T}(z^{-1})y(k) - \tilde{B}(z^{-1})\hat{R}_c w(k)|| \leq \bar{\varepsilon} < \infty$$

where $\bar{\varepsilon} = \max\{4||\tilde{Q}_1(1)||\Delta,\ 4||\tilde{Q}_2(1)||\Delta\}$.

Proof: Using the method in [24], the following properties can be given:

1) $\lim_{k\to\infty} \frac{\mu_1(k)(||e_1(k)||^2 - 16\Delta^2)}{4(1+X^T(k-1)X(k-1))} = 0$;
2) $||\hat{\Theta}_i(k) - \Theta|| \leq ||\hat{\Theta}_i(0) - \Theta||$;
3) $\lim_{k\to\infty} ||\hat{\Theta}_i(k - \hat{\Theta}_i(k-d)|| = 0$;

where d is a finite positive number and $i = 1, 2, \ldots$.

When adaptive control algorithm (52)–(54) and the linear adaptive decoupling control law (59) are applied to (32), the system input-output dynamics equations are

$$\begin{bmatrix} T(z^{-1}) + z^{-1}[\hat{F}_{1c}\cdot\hat{B}_1 - \hat{F}_{1c}\hat{B}_1] + [\hat{A}_1\cdot(\hat{\bar{H}}_{1c} + z^{-1}\hat{\bar{\bar{M}}}_{1c}) \\ -\hat{A}_1(\hat{\bar{H}}_{1c} + z^{-1}\hat{\bar{\bar{M}}}_{1c})][\tilde{B}_1\cdot(\hat{\bar{H}}_{1c} + z^{-1}\hat{\bar{\bar{M}}}_{1c}) \\ -\tilde{B}_1(\hat{\bar{H}}_{1c} + z^{-1}\hat{\bar{\bar{M}}}_{1c})] - [\tilde{Q}_1\cdot\hat{B}_1(z^{-1}) - \tilde{Q}_1\hat{B}_1(z^{-1})] \\ [\hat{A}_1\cdot\hat{F}_{1c} - \hat{A}_1\hat{F}_{1c}] \\ \hat{T}(z^{-1}) + [\tilde{Q}_1\cdot\hat{A}_1 - \tilde{Q}_1\hat{A}_1] + z^{-1}[\tilde{B}_1\cdot\hat{F}_{1c} - \tilde{B}_1\hat{F}_{1c}] \end{bmatrix} \begin{bmatrix} u(k) \\ y(k+1) \end{bmatrix} = \begin{bmatrix} \kappa_1(k) - \hat{F}_{1c}e_1(k) \\ \zeta_1(k) + \tilde{Q}_1 e_1(k+1) \end{bmatrix} \quad (63)$$

where $T(z^{-1}) = \{z^{-1}\hat{F}_{1c}(z^{-1})\hat{B}_1(z^{-1}) + \hat{A}_1(z^{-1})[\hat{\bar{H}}_{1c}(z^{-1}) + z^{-1}\hat{\bar{\bar{M}}}_{1c}(z^{-1})]\}$, $\hat{T}(z^{-1}) = \tilde{Q}_1\hat{A}_1(z^{-1}) + z^{-1}\tilde{B}_1\hat{F}_{1c}$, $\kappa_1(k) = \hat{A}_1\cdot\hat{R}_{1c}w(k)$, $\zeta_1(k) = \tilde{B}_1(z^{-1})\cdot\hat{R}_{1c}(z^{-1})w(k)$. The meaning of "$\bullet$" can be seen from [10].

When adaptive control algorithm (56)–(58) and the nonlinear adaptive decoupling control law (60) are applied to (32), the system input–output dynamics equations are (64), as shown in the bottom of the page.

$T(z^{-1}) = \{z^{-1}\hat{F}_{2c}(z^{-1})\hat{B}_2(z^{-1}) + \hat{A}_2(z^{-1})[\hat{\bar{H}}_{2c}(z^{-1}) + z^{-1}\hat{\bar{\bar{M}}}_{2c}(z^{-1})]\}$, $\hat{T}(z^{-1}) = \tilde{Q}_2\hat{A}_2(z^{-1}) + z^{-1}\tilde{B}_2\hat{F}_{2c}$, $\kappa_2(k) = \hat{A}_2\cdot\hat{R}_{2c}w(k)$, $\zeta_2(k) = \tilde{B}_2(z^{-1})\cdot\hat{R}_{2c}(z^{-1})w(k)$.

First, we prove the boundedness of the input and output signals when the linear adaptive decoupling controller (59) is used alone.

The coefficients of $\hat{A}_1(z^{-1})$ and $\hat{B}_1(z^{-1})$ are bounded for every t from (b). Thus, the coefficients of $\bar{H}_{1c}(z^{-1})$, R_{1c}, $F_{1c}(z^{-1})$, $\bar{\bar{M}}_{1c}(z^{-1})$, and $E_c(z^{-1})$ are all bounded from (46)–(48). Using the similar reasoning as in [10], the following equation can be obtained:

$$\begin{aligned} \det\left\{z^{-1}\hat{F}_{1c}\left(z^{-1}\right)\hat{B}_1\left(z^{-1}\right) + \hat{A}_1\left(z^{-1}\right)\left[\hat{\bar{H}}_{1c}\left(z^{-1}\right) + z^{-1}\hat{\bar{\bar{M}}}_{1c}\left(z^{-1}\right)\right]\right\} &= \det\left\{\tilde{B}_1\hat{F}_{1c} + z^{-1}\tilde{Q}_1\hat{A}_1\left(z^{-1}\right)\right\} \\ &= \det\left\{T\left(z^{-1}\right)\right\}. \end{aligned}$$

From 3) and (63), it follows that the coefficients of all terms in the square brackets in (63) approach zero as t goes to infinity.

$$\begin{bmatrix} T(z^{-1}) + [\hat{F}_{2c}\cdot\hat{B}_2 - \hat{F}_{2c}\hat{B}_2] + [\hat{A}_2\cdot(\hat{\bar{H}}_{2c} + z^{-1}\bar{\bar{M}}_{2c}) - \hat{A}_2(\hat{\bar{H}}_{2c} + z^{-1}\bar{\bar{M}}_{2c})] \\ \tilde{B}_2\cdot(\hat{\bar{H}}_{2c} + z^{-1}\bar{\bar{M}}_{2c}) - \tilde{B}_2(\hat{\bar{H}}_{2c} + z^{-1}\bar{\bar{M}}_{2c})] - [\tilde{Q}_2\cdot\hat{B}_2(z^{-1}) - \tilde{Q}_2\hat{B}_2(z^{-1})] \\ [\hat{A}_2\cdot\hat{F}_{2c} - \hat{A}_2\hat{F}_{2c}] - [\hat{F}_{2c}\cdot\hat{A}_2(z^{-1}) - \hat{F}_{2c}\hat{A}_2(z^{-1})] \\ \hat{T}(z^{-1}) + z^{-1}[\tilde{B}_2\cdot\hat{F}_{2c} - \tilde{B}_2\hat{F}_{2c}] + [\tilde{Q}_2\cdot\hat{A}_2(z^{-1}) - \tilde{Q}_2\hat{A}_2(z^{-1})] \end{bmatrix} \begin{bmatrix} u(k) \\ y(k+1) \end{bmatrix}$$

$$= \begin{bmatrix} \kappa_2(k) - \hat{F}_{2c}e_2(k) - [\hat{A}_2\cdot\hat{E}_c - \hat{A}_2\hat{E}_c]v(k-1) - [\hat{A}_2\hat{E}_c + z^{-1}\hat{F}_{2c}]\hat{v}(k-1) \\ \zeta_2(k) + \tilde{Q}_2 e_2(k+1) - z^{-1}[\tilde{B}_2\cdot\hat{E}_c(z^{-1}) - \tilde{B}_2\hat{E}_c(z^{-1})]\hat{v}(k) - [z^{-1}\tilde{B}_2\hat{E}_c(z^{-1}) - \tilde{Q}_2]\hat{v}(k) \end{bmatrix} \quad (64)$$

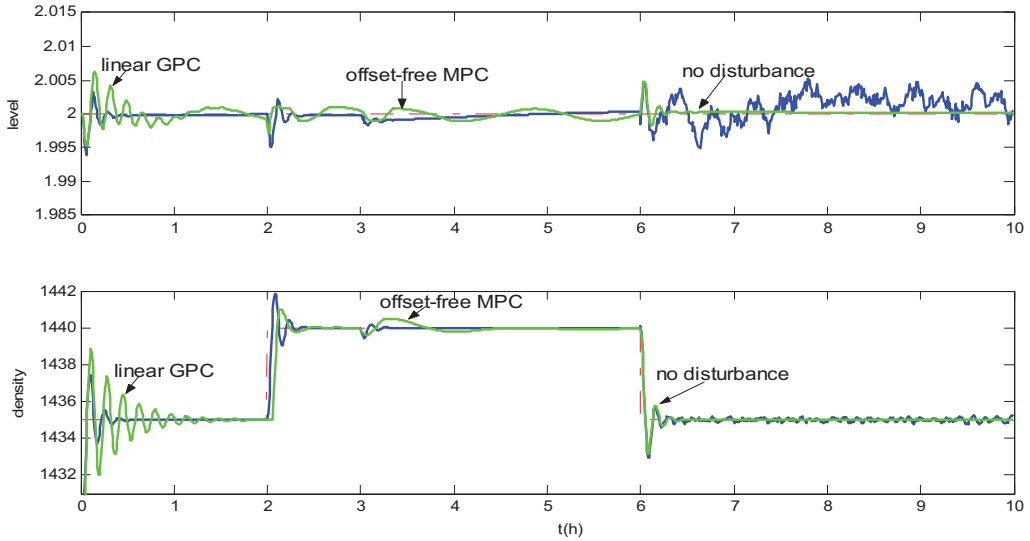

Fig. 6. Response of level and product density.

Thus, the closed-loop systems (63) are exponentially stable. By using the boundedness of the interference input $w(t)$, there exist positive constants c_1, c_2, c_3, and c_4 satisfying

$$||y(k)|| \le c_1 + c_2 \max_{0\le\tau\le k} ||e_1(k)||$$
$$||u(k)|| \le c_3 + c_4 \max_{0\le\tau\le t} ||e_1(k)||.$$

Since $X(k-1) = [-y^T(k-1), \ldots, -y^T(k-n_a), u^T(k-1), \ldots, u^T(k-n_b-1)]^T$, there exist positive constants c_5, and c_6 satisfying

$$||X(k-1)|| \le c_5 + c_6 \max_{0\le\tau\le k} ||e_1(k)||. \tag{65}$$

Then boundedness of $X(k-1)$ can be obtained from the boundedness of $e_1(k)$. Using the similar methods [28], the boundedness of $e_1(k)$ can be proved by the contradiction. Thus, we obtain that $X(K-1)$ is bounded, i.e., the input and output signals of the closed-loop system are bounded when the linear adaptive decoupling control law (59) is used alone.

Secondly, we prove the boundedness of the input and output signals when the adaptive algorithm (52)–(54) and (56)–(58) and the switching mechanism (61) are applied to the system. Using (62), the second term in (61) is always bounded, and combine the property 1), it can be obtained that $J_1(k)$ is bounded. For $J_2(k)$, there exist two cases.

1) $J_1(k) \le J_2(k)$.

In this case, the linear adaptive decoupling controller (59) will be applied to system by the switching mechanism. From the analysis above, the closed-loop system is stable.

2) $J_2(k) \le J_1(k)$.

Using the switching mechanism, the nonlinear adaptive decoupling controller (60) will be used to control the system. According to (64) and boundedness of the interference input $w(k)$ and $\hat{v}(k)$, and using the similar way, there exist positive constants c_7, and c_8 such that

$$||X(k-1)|| \le c_7 + c_8 \max_{0\le\tau\le k} ||e_2(k)||. \tag{66}$$

On the other hand, since $J_1(k)$ is always bounded and $J_2(k) < J_1(k)$, it can be seen that $J_2(k)$ is bounded. Combining the switching function (61) with the boundedness of $J_2(k)$, we have

$$\lim_{t\to\infty} \frac{\mu_2(k)(||e_2(k)||^2 - 16\Delta^2)}{4(1 + X^{\mathrm{T}}(k-1)X(k-1))} = 0. \tag{67}$$

By using (66) and (67), as well as [19, Lemma 3.1], we can obtain that $X(k-1)$ is bounded, i.e., the input and output signals of the closed-loop switching system is bounded.

Finally, we analyze the convergence of the closed-loop system. From (67), and the boundedness of $X(k-1)$, we obtain that the estimation error of the switching system $e(k) = e_1(k)$ or $e_2(k)$ should satisfy

$$\lim_{k\to\infty} \frac{\mu(k)(||e_i(k)||^2 - 16\Delta^2)}{4(1 + X(k-1)^{\mathrm{T}}X(k-1))} = 0. \tag{68}$$

From (65)–(67), it can be obtained that

$$\lim_{k\to\infty} \mu(k)(||e_i(k)||^2 - 16\Delta^2) = 0.$$

According to the definition of $\mu_j(k)$ and (68), it can be obtained that

$$\lim_{k\to\infty} \sup ||e_1(k)|| \le 4\Delta. \tag{69}$$

When the linear adaptive decoupling controller (59) is applied to the system, it can be obtained that

$$\lim_{k\to\infty} |\hat{T}(z^{-1})y(k) - \tilde{B}_1(z^{-1})\hat{R}_{1c}w(k)|| = \lim_{t\to\infty} ||\tilde{Q}_1(z^{-1})e_1(k)||.$$

Then the following equation can be obtained:

$$\lim_{k\to\infty} ||\hat{T}(z^{-1})y(k) - \tilde{B}_1(z^{-1})\hat{R}_{1c}w(k)|| \le 4||\tilde{Q}_1(1)||\Delta.$$

Similarly, when the nonlinear adaptive decoupling controller (60) is applied to the system, it can be obtained that the generalized tracking error of the closed-loop switching system should satisfy

$$\lim_{k\to\infty} ||\hat{T}(z^{-1})y(k) - \tilde{B}_2(z^{-1})\hat{R}_{2c}w(k)|| \le 4||\tilde{Q}_2(1)||\Delta.$$

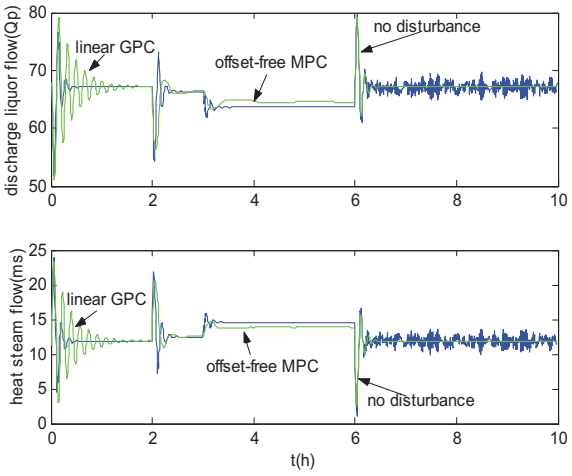

Fig. 7. Corresponding control inputs.

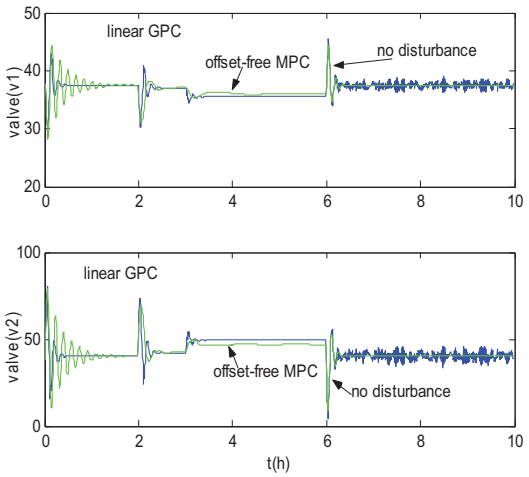

Fig. 8. Corresponding valve opening.

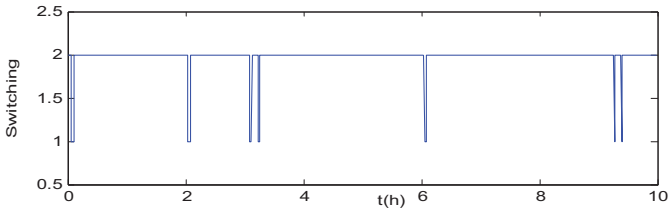

Fig. 9. Switching sequence: 1 denotes the linear adaptive control and 2 denotes the neural network nonlinear adaptive control.

Define $\bar{\varepsilon} = \max\{4||\tilde{Q}_1(1)||\Delta,\ 4||\tilde{Q}_2(1)||\Delta\}$, then whether the linear adaptive decoupling controller or the nonlinear adaptive decoupling controller is applied, the generalized tracking error of the closed-loop system satisfies

$$\lim_{k\to\infty}||\bar{e}(k)|| = \lim_{k\to\infty}||\hat{T}(z^{-1})y(k) - \tilde{B}(z^{-1})\hat{R}_c w(k)|| \le \bar{\varepsilon} < \infty.$$

The proof is thus completed.

Remark 3: Theorem 1 guarantees the BIBO stability of the closed-loop system. It is should be noted that the proposed method can not only deal with the strong nonlinear dynamics but also cope with the strong couplings and uncertain parameters in the forced-circulation system.

V. Simulation Results

Simulation results presented here are achieved by applying the proposed method to the forced-circulation evaporation system. While (22) is used as the nonlinear model for the simulation, discrete-time model given by (32) is used as the controller design model. Using the least-squares identification algorithm, the initial design model can be obtained around the nominal operating point as follows:

$$\hat{A}(z^{-1}) = \begin{bmatrix} 1 - 1.9894z^{-1} + 0.9847z^{-2} & 0 \\ 0 & 1 - 1.9845z^{-1} + 0.9890z^{-2} \end{bmatrix}$$

$$\hat{B}(z^{-1}) = 1\times 10^{-2}\begin{bmatrix} -0.01883 + 0.01867z^{-1} & -0.02429 + 0.02408z^{-1} \\ -1.3189 + 1.30984z^{-1} & 0.5199 - 0.0518z^{-1} \end{bmatrix}$$

where the system orders are $n_a = 2$, $n_b = 1$. In this case $\lambda = I$, $N = 3$, and $Q_0 = \text{diag}\{0.01\ 0.03\ 1\ 1\ 1\ 1\}$ are selected, and the parameters of the switching criterion are chosen to be $\alpha = 1$, $N = 2$, and $\Delta = 0.3$. Two groups of multilayer neural networks are adopted. Three illustrative examples are provided to demonstrate the performance of the proposed nonlinear adaptive decoupling switching control. The examples will show the following three scenarios: namely the effect of setpoint changes, parametric uncertainties, and the load disturbances on the control system.

The experiments are designed as follows. The level setpoint of the forced-circulation system evaporator does not change during the experiment process. In order to study the tracking performance of the adaptive decoupling switching controller, the product density is changed from 1429.4 to 1435 kg/m^3 at t = 0–2 h. For comparison, the linear GPC control strategy is adopted in this process. The product density is changed from 1435 to 1440 kg/m^3 at t = 2–5 h, and the effect of changes of the specific heat of the liquor are simulated during the process, the specific heat of the liquor is varied from 3.61 to 3.63 kJ/(kg· kJ/(kg·°C) at t = 3 h. The offset-free MPC [28], [29] strategy is adopted for the comparison. Effect of the external disturbance are simulated during t = 5–7 h, where a random bounded disturbance is added to the feed flow rate and the feed density at t = 5, the ranges of the feed flow rate and the feed density are 76–84 m^3/h and 1361–1369 kg/m^3, respectively. The setpoint of product density changes from 1440 to 1435 kg/m^3. For comparison, the situation of no external disturbances is also shown (__. No disturbance __. External disturbances) in this brief.

The simulation results of the setpoint tracking are shown in Figs. 6–9. It can be seen that the system performance is not good for the linear GPC strategy. The product density reaches the steady-state very slowly, whereas the level features large fluctuations. The nonlinear adaptive decoupling switching controller can reduce the coupling between the level loop and the density loop.

In the presence of the uncertain parameters, the level of the evaporator undergoes less fluctuations and the product density can track the setpoint quickly. It is worth noting that the

proposed method can reduce the impact of the uncertainties on the system. The level and the density are quickly steered to the setpoint when the disturbance occurs. The offset-free MPC is applied to the forced-circulation system simultaneously [29], [30]. As it can be seen from Fig. 6, the offset-free MPC can track the setpoints very quickly and can eliminate the steady-state error. Compared with offset-free MPC method, the proposed method can achieve slight better control performance. Moreover, in order to eliminate the steady-state error, the offset-free MPC should obtain the unmeasured disturbance model and estimator. At the same time, the augmented system should be detectable and should satisfy certain conditions [29]. Thus, the adaptive method is relatively simple to handle the model parameters uncertainties problem when compared with the offset-free MPC method.

In the presence of the external disturbance, it can be seen that the dynamic behaviors of both level and produce density under the external disturbances can achieve good control performance. Therefore, it can be concluded that the nonlinear adaptive decoupling switching control method is highly robust for the actual forced-circulation evaporation process.

VI. Conclusion

A nonlinear adaptive decoupling switching control strategy has been proposed in this brief for the forced-circulation system of the alumina production. The plant dynamics are shown to be multivariable, strongly coupled, nonlinear, and uncertainties. It has been shown that the proposed method can not only mitigate nonlinearities and reduce the interactions between the density control and the level control loops, but also improve the transient performance and the evaporation efficiency for the forced-circulation system. Since the forced-circulation evaporation system is used widely in chemistry, metallurgy, paper making, food and salt processes, etc., the proposed method has a wide application and can be applied to these industry processes with minor modification.

References

[1] L. C. To, M. O. Tadé, and G. P. Le, "Implementation of a differential geometric nonlinear controller on an industrial evaporator system," *Control Eng. Pract.*, vol. 6, no. 11, pp. 1309–1319, 1998.

[2] L. C. To, M. O. Tadé, M. Kraetzl, and G. P. L. Page, "Nonlinear control of a simulated industrial evaporation process," *J. Process Control*, vol. 5, no. 3, pp. 173–182, 1995.

[3] K. M. Kam and M. O. Tade, "Simulated Nonlinear control studies of five-effect evaporator models," *Comput. Chem. Eng.*, vol. 23, nos. 11–12, pp. 1795–1810, 2000.

[4] P. Quaak, M. P. C. M. van Wijck, and J. J. Van Haren, "Comparison of process identification and physical modelling for falling-film evaporators," *Food Control*, vol. 5, no. 2, pp. 73–82, 1994.

[5] S. T. Lahtinen, "Identification of fuzzy controller for use with a falling-film evaporator," *Food Control*, vol. 12, no. 3, pp. 175–180, 2001.

[6] J. E. Lozano, M. P. Elustondo, and J. A. Romagnoli, "Control studies in an industrial apple juice evaporator," *J. Food Sci.*, vol. 49, no. 6, pp. 1422–1427, 1984.

[7] G. P. Rangaiah, "Nonlinear model predictive control of an industrial four-stage evaporator system via simulation," *Chem. Eng. Comput. J.*, vol. 87, no. 3, pp. 285–299, 2002.

[8] P. E. McDermott and D. A. Mellichamp, "A decoupling pole placement self-tuning controller for a class of multivariable process," *Opt. Control Appl. Methods*, vol. l7, no. 1, pp. 55–79, 1986.

[9] S. J. Lang, X. Y. Gu, and T. Y. Chai, "A multivariable generalized self-tuning controller with decoupling design," *IEEE Trans. Autom. Control*, vol. 31, no. 5, pp. 474–477, May 1986.

[10] T. Y. Chai, "Direct adaptive decoupling control for general stochastic multivariable systems," *Int. J. Control*, vol. 51, no. 4, pp. 885–909, 1990.

[11] T. P. Zhang and S. S. Ge, "Adaptive neural network tracking control of MIMO nonlinear systems with unknown dead zones and control directions," *IEEE Trans. Neural Netw.*, vol. 20, no. 3, pp. 483–497, Mar. 2009.

[12] B. Chaudhuri, R. Majumder, and B. C. Pal, "Application of multiple-model adaptive control strategy for robust damping of interarea oscillations in power system," *IEEE Trans. Control Syst. Technol.*, vol. 12, no. 5, pp. 727–736, Sep. 2004.

[13] N. V. Q. Hung, H. D. Tuan, T. Narikiyo, and P. Apkarian, "Adaptive control for nonlinearly parameterized uncertainties in robot manipulators," *IEEE Trans. Control Syst. Technol.*, vol. 16, no. 3, pp. 458–468, May 2008.

[14] K. P. Tee, S. S. Ge, and F. E. H. Tay, "Adaptive neural network control for helicopters in vertical flight," *IEEE Trans. Control Syst. Technol.*, vol. 16, no. 4, pp. 753–762, Jul. 2008.

[15] Y. Fu and T. Y. Chai, "Intelligent decoupling control of nonlinear multivariable systems and its application to a wind tunnel system," *IEEE Trans. Control Syst. Technol.*, vol. 17, no. 6, pp. 1376–1384, Nov. 2009.

[16] Q. Bi, W. J. Cai, E. L. Lee, Q. G. Wang, C.-C. Hangb, and Y. Zhang, "Robust identification for first-order plus dead-time model from step response," *Control Eng. Pract.*, vol. 7, no. 1, pp. 71–77, 1999.

[17] S.-Y. Li, W.-J. Cai, H. Mei, and Q. Xiong, "Robust decentralized parameter identification for two-input two-output process from closed-loop step responses," *Control Eng. Pract.*, vol. 13, no. 4, pp. 519–531, 2005.

[18] D. C. Aliprantis, S. D. Sudhoff, and B. T. Kuhn, "Genetic algorithm-based parameter identification of a hysteretic brushless exciter model," *IEEE Trans. Energy Convers.*, vol. 21, no. 1, pp. 148–154, Mar. 2006.

[19] Y. Leehter and W. A. Sethares, "Nonlinear parameter estimation via the genetic algorithm," *IEEE Trans. Signal Process.*, vol. 42, no. 4, pp. 927–935, Apr. 1994.

[20] W. Tan, H. J. Marquez, T. Chen, and J. Liu, "Analysis and control of a nonlinear boiler-turbine unit," *J. Process Control*, vol. 15, no. 8, pp. 883–891, 2005.

[21] J. Du, C. Song, and P. Li, "Application of gap metric to model bank determination in multi-linear model approach," *J. Process Control*, vol. 19, no. 2, pp. 231–240, 2009.

[22] K. M. Kam, "Simulation and implementation of nonlinear control systems for mineral processes," Ph.D. dissertation, Curtin Univ. Technol., School Chem. Eng., Australia, 2000.

[23] L. C. To, "Nonlinear control techniques in alumina refineries," Ph.D. dissertation, School Chem. Eng., Curtin Univ. Technol., Bentley, Australia, 1996.

[24] Y. G. Wang, T. Y. Chai, J. Fu, Y. J. Zhang, and Y. Fu, "Adaptive decoupling switching control based on generalized predictive control," *IET Control Theory Appl.*, to be published.

[25] T. Y. Chai, L. Y. Zhai, and H. Yue, "Multiple models and neural networks based decoupling control of ball mill coal-pulverizing systems," *J. Process Control*, vol. 21, no. 3, pp. 351–366, 2011.

[26] S. S. Ge, T. H. Lee, G. Y. Lj, and J. Zhang, "Adaptive NN control for a class of discrete-time nonlinear system," *Int. J. Control*, vol. 76, no. 4, pp. 334–354, 2003.

[27] L. J. Chen and K. S. Narendra, "Nonlinear adaptive control using neural networks and multiple models," *Automatica*, vol. 37, no. 8, pp. 1245–1255, 2001.

[28] G. C. Goodwin, P. J. Ramadge, and P. E. Caines, "Discrete-time mutivariable adaptive control," *IEEE Trans. Autom. Control*, vol. 25, no. 3, pp. 449–456, Jun. 1980.

[29] K. R. Muske and T. A. Badgwell, "Disturbance modeling for offset-free linear model predictive control," *J. Process Control*, vol. 12, no. 5, pp. 617–632, 2002.

[30] G. Pannocchia and J. B. Rawlings, "Disturbance models for offset-free model predictive control," *AICHE J.*, vol. 49, no. 2, pp. 426–437, 2003.